

Investigating Galaxy-Filament Alignments in Hydrodynamic Simulations using Density Ridges

Yen-Chi Chen,^{1,3*} Shirley Ho,^{2,3} Ananth Tenneti,^{2,3} Rachel Mandelbaum,^{2,3}
 Rupert Croft,^{2,3} Tiziana DiMatteo,^{2,3} Peter E. Freeman,^{1,3}
 Christopher R. Genovese,^{1,3} Larry Wasserman^{1,3}

¹*Department of Statistics, Carnegie Mellon University, Pittsburgh, PA 15213, USA*

²*Department of Physics, Carnegie Mellon University, Pittsburgh, PA 15213, USA*

³*McWilliams Center for Cosmology, Department of Physics, Carnegie Mellon University, Pittsburgh, PA 15213, USA*

13 June 2021

ABSTRACT

In this paper, we study the filamentary structures and the galaxy alignment along filaments at redshift $z = 0.06$ in the MassiveBlack-II simulation, a state-of-the-art, high-resolution hydrodynamical cosmological simulation which includes stellar and AGN feedback in a volume of $(100 \text{ Mpc}/h)^3$. The filaments are constructed using the subspace constrained mean shift (SCMS; Ozertem & Erdogmus (2011) and Chen et al. (2015a)). First, we show that reconstructed filaments using galaxies and reconstructed filaments using dark matter particles are similar to each other; over 50% of the points on the galaxy filaments have a corresponding point on the dark matter filaments within distance $0.13 \text{ Mpc}/h$ (and vice versa) and this distance is even smaller at high-density regions. Second, we observe the alignment of the major principal axis of a galaxy with respect to the orientation of its nearest filament and detect a $2.5 \text{ Mpc}/h$ critical radius for filament's influence on the alignment when the subhalo mass of this galaxy is between $10^9 M_\odot/h$ and $10^{12} M_\odot/h$. Moreover, we find the alignment signal to increase significantly with the subhalo mass. Third, when a galaxy is close to filaments (less than $0.25 \text{ Mpc}/h$), the galaxy alignment toward the nearest galaxy group depends on the galaxy subhalo mass. Finally, we find that galaxies close to filaments or groups tend to be rounder than those away from filaments or groups.

Key words: (cosmology:) large-scale structure of Universe, hydrodynamics

1 INTRODUCTION

Weak gravitational lensing by large-scale structure of the Universe, commonly known as cosmic shear, is a promising technique to constrain cosmological parameters. It is among the key science cases of various ongoing and upcoming surveys, such as the Kilo-Degree Survey (KiDS¹), Hyper Suprime Cam (HSC²), Dark Energy Survey (DES³), Large Synoptic Survey Telescope (LSST⁴), Euclid⁵ and the Wide-Field Infrared Survey Telescope (WFIRST⁶). Theoretically, it provides valuable information on both the geometry and

structure growth of the Universe without assumptions on the relationship between the luminous and dark matter; see e.g. Hoekstra et al. (2002); Van Waerbeke et al. (2005); Jarvis et al. (2006); Schrabback et al. (2010); Lin et al. (2012); Heymans et al. (2012); Jee et al. (2013); Huff et al. (2014). If systematics can be sufficiently controlled for future missions, cosmic shear has the potential to be the most constraining cosmological probe, thus understanding and controlling systematics in the weak lensing measurements needs to improve significantly over the next few years for its potential to come to fruition with large data volumes in these upcoming surveys.

Cosmic shear is typically measured through two-point correlations of observed galaxy ellipticities. In the weak lensing regime, the observed ellipticity of a galaxy is the sum of its intrinsic ellipticity ϵ_t and gravitational shear γ : $\epsilon_{\text{obs}} \approx \epsilon_t + \gamma$. When the intrinsic shapes of galaxies are spatially correlated, these intrinsic alignment (IA) correla-

* E-mail: yenchic@andrew.cmu.edu

¹ <http://kids.strw.leidenuniv.nl/>

² <http://www.naoj.org/Projects/HSC/>

³ <http://www.darkenergysurvey.org/>

⁴ <http://www.lsst.org/lsst/>

⁵ <http://sci.esa.int/euclid/>

⁶ <http://wfirst.gsfc.nasa.gov/>

tions can contaminate the gravitational shear signal and lead to biased measurements if not properly removed or modeled. Since early work establishing its potential effects (Croft & Metzler 2000; Heavens et al. 2000; Catelan et al. 2001; Crittenden et al. 2001), IA has been examined through observations (e.g., Hirata et al. 2007; Joachimi et al. 2011; Blazek et al. 2012; Singh & Mandelbaum 2014), analytic modeling, and simulations (e.g., Schneider et al. 2012; Tenneti et al. 2014, 2015). See Troxel & Ishak (2014); Joachimi et al. (2015), and references therein, for recent reviews.

To create a fully predictive model of IA would require the understanding of the complex processes involved in the formation and evolution of galaxies and their dark matter halos, as well as how these processes couple to large-scale environment. The shapes of elliptical, pressure-supported galaxies are often assumed to align with the surrounding dark matter halos, which are themselves aligned with the stretching axis of the large-scale tidal field (Catelan et al. 2001; Hirata & Seljak 2004, 2010). This tidal alignment model leads to shape alignments that scale linearly with fluctuations in the tidal field, and it is thus sometimes referred to as “linear alignment”, although nonlinear contributions may still be included (Bridle & King 2007; Blazek et al. 2011, 2015). As for spiral galaxies, where angular momentum is likely the primary factor in determining galaxy orientation, IA modeling is typically based on tidal torquing theory, leading to a quadratic dependence on tidal field fluctuations (Pen et al. 2000; Catelan et al. 2001; Hui & Zhang 2002; Lee & Pen 2008), although on sufficiently large scales, the contribution linear in the tidal field may become dominant.

Filaments in the cosmic web play a key role in the large-scale tidal field since they are related to the gradient and the Hessian matrix of the matter density field (Hahn et al. 2007a,b; Sousbie et al. 2008; Forero-Romero et al. 2009; Aragón-Calvo et al. 2010; Cautun et al. 2013). As a result, it is expected that filaments would affect the shapes and alignments of their nearby galaxies. There is evidence for anti-alignment between the galaxy spin orientation of disk galaxies and the direction of nearby filaments (Libeskind et al. 2013; Tempel et al. 2013; Tempel & Libeskind 2013; Aragon-Calvo & Yang 2014; Dubois et al. 2014; Welker et al. 2014; Laigle et al. 2015; Zhang et al. 2015), and an alignment between galaxy shape and the orientation of the nearest filament (Altay et al. 2006; Zhang et al. 2009; Tempel & Libeskind 2013; Zhang et al. 2013). Other evidence also indicates that direction of a galaxy pair (Tempel & Tamm 2015) and the alignment of satellite galaxies toward their host galaxies (Tempel et al. 2015) are dependent on their nearby filaments. The effect of filaments on intrinsic galaxy shapes is worth studying since filaments are expected to trace the tidal fields directly and yet the current theoretical model for IA only includes halos but does not explicitly include filaments; see e.g. Schneider & Bridle (2010).

One can, in principle, test and constrain IA models and marginalize over free parameters in specific models; this process could be improved in the quasilinear and nonlinear regime via the tighter priors on model parameters that we could obtain with a 3D filament map of the universe which overlaps with sources in the weak lensing fields. In this paper, we apply the subspace constrained mean shift (SCMS) filament finder to the source density in a cosmological hydrodynamic simulation to test whether we can use filaments

as a tool to understand the relationship of galaxy alignments with the large-scale density field.

We start with a brief introduction about density ridges, the model for filaments we are using, in § 2 and describe the MassiveBlack-II Simulation we applied in § 3. Then we describe our main results in § 4 and our conclusions in § 5.

2 DENSITY RIDGES AS FILAMENTS

We detect filaments through SCMS introduced in Ozertem & Erdogmus (2011); Chen et al. (2015a). SCMS is a gradient-based method that detects filaments as “galaxy density ridges”.

Essentially, filaments from SCMS are defined as follows. Given galaxies located at $X_1, \dots, X_n \in \mathbb{R}^3$, the smoothed density field (also known as the kernel density estimator) is

$$p(x) = \frac{1}{nb^3} \sum_{i=1}^n K\left(\frac{|x - X_i|}{b}\right), \quad (1)$$

where K is a Gaussian and b is the smoothing bandwidth that controls the amount of smoothing on each particle. In this paper, we apply $b = 1$ Mpc/h. Note that the density field p does not incorporate any boundary condition at the edge of the simulation box. Let $g(x) = \nabla p(x)$, $H(x) = \nabla \nabla p(x)$ be the gradient and Hessian matrix of $p(x)$. Ridges of $p(x)$ are the collection of points

$$F = \{x : v_j(x) \cdot g(x) = 0, \lambda_2(x) < 0, j = 2, 3\}, \quad (2)$$

where $v_j(x)$, $\lambda_j(x)$ are the j -th eigenvector/value for $H(x)$. See Figure 1 for an example about density ridges. More properties of ridges of a function can be found in Eberly (1996); Ozertem & Erdogmus (2011); Genovese et al. (2014); Chen et al. (2014, 2015c).

Intuitively, at a point on the ridge, the gradient is the same as $v_1(x)$, the eigenvector corresponds to the largest eigenvalue, and the density curves downward sharply in directions orthogonal to the gradient. When p is smooth and the *eigen-gap*

$$\beta(x) = \lambda_1(x) - \lambda_2(x) \quad (3)$$

is positive, the ridges have the properties of filaments (Chen et al. 2015c). That is, F decomposes into a set of smooth curve-like structures with high-density. Since the ridges are smooth, for any point $x \in F$, the orientation of ridges at x , denoted as $\mu_{\text{Ridge}}(x)$, is well-defined.

3 MASSIVEBLACK-II SIMULATION

In this work, we detect filaments in the MassiveBlack-II (MBII) hydrodynamic simulation (Khandai et al. 2015), and study the alignments of the shapes of stellar matter components in galaxies with the filaments. MB-II is a state-of-the-art, high-resolution cosmological hydrodynamic simulation performed in a cubic periodic box of size 100 Mpc/h on a side. The simulations have been performed with the code P-GADGET, which is a hybrid version of the parallel code GADGET2 (Springel et al. 2005) that has been modified and upgraded to run on Petaflop-scale supercomputers. MBII includes the physics of multiphase interstellar medium (ISM) model with star formation (Springel & Hernquist 2003),

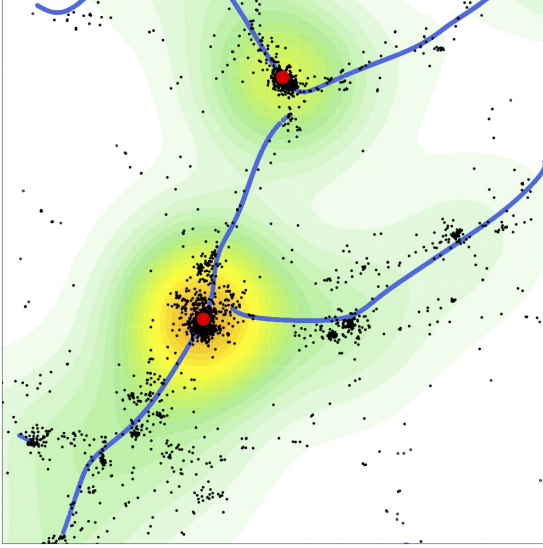


Figure 1. Illustration of density ridges (blue curves) in a density field. Each black dot is a subhalo and the big red dots are galaxy groups. The color from white-green-yellow-orange denotes the density induced by smoothing the subhalos. Note that this 2-D figure is for illustration; our analysis is applied to 3-D data.

black hole accretion and associated feedback processes (Di Matteo et al. 2008, 2012) in addition to gravity and hydrodynamics. This simulation has been run from $z = 159$ to $z = 0.06$ using $N_{\text{part}} = 2 \times 1792^3$ dark matter and gas particles with a gravitational smoothing length, $\epsilon = 1.85 \text{ kpc}/h$ in comoving units. The mass of each dark matter particle is $m_{\text{DM}} = 1.1 \times 10^7 M_{\odot}/h$ and the initial mass of a gas particle is $m_{\text{gas}} = 2.2 \times 10^6 M_{\odot}/h$. The cosmological parameters in the simulation chosen according to WMAP7 (Komatsu et al. 2011) are as follows: amplitude of matter fluctuations $\sigma_8 = 0.816$, spectral index $n_s = 0.96$, mass density parameter $\Omega_m = 0.275$, cosmological constant density parameter $\Omega_{\Lambda} = 0.725$, baryon density parameter $\Omega_b = 0.046$, and Hubble parameter $h = 0.702$.

To generate halo catalogs, the friend-of-friends (FOF) halo finder algorithm (Davis et al. 1985) is used with a linking length of 0.2 times the mean interparticle separation. The SUBFIND code (Springel et al. 2001) is used on the halo catalogs to generate subhalo catalogs. Here, subhalos are defined as locally overdense, self-bound particle groups which consist of at least 20 gravitationally bound particles. However, to ensure that the measured shape of a galaxy is reliable, we restrict our galaxy sample to those subhalos with at least 500 star particles. This is based on the convergence tests in Tenneti et al. (2014).

3.1 Shapes of galaxies

In this paper, we use the shapes of the stellar components of galaxies in MBII which are calculated in Tenneti et al. (2015) to quantify intrinsic alignments of galaxies. Here, we give a brief description of the method adopted to calculate these shapes. The shapes of galaxies are modeled as ellipsoids in three dimensions by the eigenvalues and eigenvectors

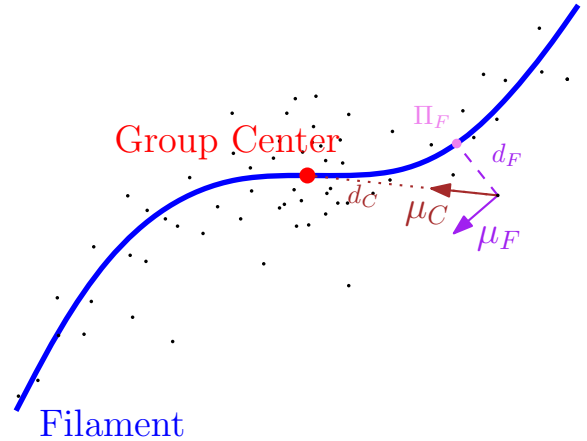


Figure 2. Example of μ_C, μ_F, d_C, d_F . The big red dot denotes a galaxy group, the blue curve is the filament, and the small black points are galaxies. For a given point (galaxy), the brown arrow is μ_C and the purple arrow is μ_F . The length of the dotted brown line is d_C and of the dashed purple line is d_F . Note that the projected point onto the filament is the pink point.

obtained from the eigen-decomposition of the reduced inertia tensor. We consider all the star particles belonging to the subhalo in the calculation of the inertia tensor. The eigenvectors of the inertia tensor are denoted as μ_1, μ_2 , and μ_3 with the corresponding eigenvalues being λ_a, λ_b , and λ_c , where $\lambda_a > \lambda_b > \lambda_c$. The lengths of the principal axes of the ellipsoid (a, b, c), which are represented by these eigenvectors, are given by square roots of the eigenvalues ($\sqrt{\lambda_a}, \sqrt{\lambda_b}, \sqrt{\lambda_c}$). We can now define the intermediate-to-major axis ratio (q) and the minor-to-major axis ratio (s) as

$$q = \frac{b}{a}, \quad s = \frac{c}{a} \quad (4)$$

Note that an iterative procedure is adopted in calculating the shapes such that the axis ratios converge. For additional details regarding the iterative method, see Tenneti et al. (2015).

For each galaxy, we have two intrinsic quantities: the number of star particles n and the total mass of this subhalo M (subhalo mass). Throughout this paper, we use only subhalo mass.

3.2 Large-Scale Structure

In our analysis, we define galaxy groups as those subhalos with subhalo mass $> 10^{13} M_{\odot}/h$. This gives 315 galaxy groups, which corresponds to a comoving number density $3.15 \times 10^{-4} (h/\text{Mpc})^3$. Let C and F denote the collection of all groups (of galaxies) and filaments. Given any galaxy located at x (x is the 3D position in the box), let $\Pi_C(x) \in C$ and $\Pi_F(x) \in F$ be the ‘projected’ point onto the nearest group/filament. Namely, $\Pi_C(x)$ (or $\Pi_F(x)$ respectively) is the point in C (or F) whose distance to x is smallest among all points in C (or F). In general, this projection is unique (although some regions may have non-unique projection, the probability that a galaxy falls within these regions is 0). We then define the associated direction to the nearest group and

Notation	Definition	Type	Remark
n	Number of star particles	Integer	> 500
M	Halo mass	Scalar	
d_C	Distance to the nearest galaxy group	Scalar	
d_F	Distance to the nearest filament	Scalar	
μ_C	Direction to the nearest galaxy group	Vector	
μ_F	Orientation of the nearest filament	Vector	
q	First and second principal axis ratio	Scalar	$\in [0, 1]$
s	First and third principal axis ratio	Scalar	$\in [0, 1]$
μ_1	First principal axis	Vector	
μ_2	Second principal axis	Vector	
μ_3	Third principal axis	Vector	

Table 1. Table of quantities associated with a galaxy.

to the nearest filament as

$$\mu_C(x) = \frac{\Pi_C(x) - x}{|\Pi_C(x) - x|} \quad (5)$$

$$\mu_F(x) = \mu_{\text{Ridge}}(\Pi_F(x)). \quad (6)$$

Note that μ_C is the direction *toward* the nearest galaxy group while μ_F is the direction *of* the nearest filaments. We also define the projection distances $d_C(x) = |\Pi_C(x) - x|$ and $d_F(x) = |\Pi_F(x) - x|$. Namely, for a galaxy at position x , $\mu_C(x)$ is the direction from this galaxy to the nearest galaxy group. And $\mu_F(x)$ is the orientation of the nearby filament. Figure 2 illustrates all the above quantities in a 2-D picture.

4 RESULTS

4.1 Agreement of Filaments from Galaxies versus Dark Matter Particles

To establish the promise of recovering filaments tracing dark matter particles using only galaxies, we first study the similarity for filaments obtained by using galaxies only versus using dark matter particles. The dark matter particles are from a random subsample with size 400,000, which is approximately the same order as the number of subhalos we have ($\sim 500,000$). In Figure 3, we show the difference between the two filament catalogues. Since both catalogues contain points on the filaments, the difference is computed using projected distance between points from two catalogues (Chen et al. 2015b). To be more specific, let \mathcal{F}_D and \mathcal{F}_G be the collection of points on the filaments from dark matter particles and from galaxies. Then for each point in \mathcal{F}_D , we find its nearest distance to any member of \mathcal{F}_G . This gives a distance value (also known as projected distance) to each point in \mathcal{F}_D . Similarly, for every point in \mathcal{F}_G , we can find the corresponding projected distance to \mathcal{F}_D so that we will assign a distance value to each element of \mathcal{F}_G . The distribution of all the distance values in \mathcal{F}_D and \mathcal{F}_G provides the information about similarity between these two filament catalogues. If they are similar, this distribution will be concentrated around 0. On the other hand, if the two catalogues are different, this distribution will spread out. Note that we have tried a random sample with size 800,000 and the result remains similar.

According to Figure 3, we see that the two catalogues are similar to each other; more than 50% of the points on

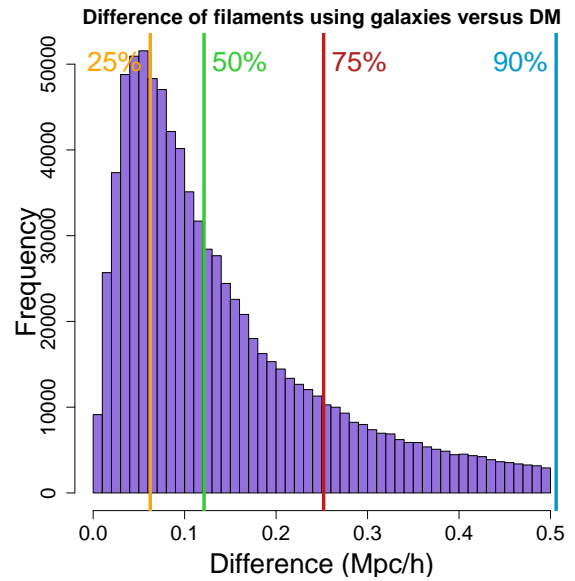


Figure 3. Agreement of filaments detected using galaxies versus using dark matter particles. We apply our filament finder to both galaxies and dark matter particles and then compare the difference between the two corresponding filament catalogues. This picture shows the distribution of difference in filament position. The four color bars denote the quantile values of 25%, 50%, 75% and 90%. The difference for filaments recovered from galaxies and dark matter particles is small.

filaments differ at a distance less than 0.13 Mpc/h and about 90% of them differ at the distance less than 0.5 Mpc/h.

We also study the agreement for the two catalogues at different densities. For each point on the filaments, we assign a density value to them by using the distance to the 1000-th nearest dark matter particles (Figure 4). The 1000 is chosen arbitrarily; we have tried other values and the result remains similar. The inverse of this distance is an effective density (at overdense regions, this distance is small while at void region, this distance is large). We then rank points on filaments according to their densities and plot the distribution of difference under different density ranking categories. The high-density filaments are those whose density ranking is among the top 10% (red) and top 25% (orange). The low density filaments are those whose density ranking is in the bottom 25% (green) and bottom 10% (blue). The result is

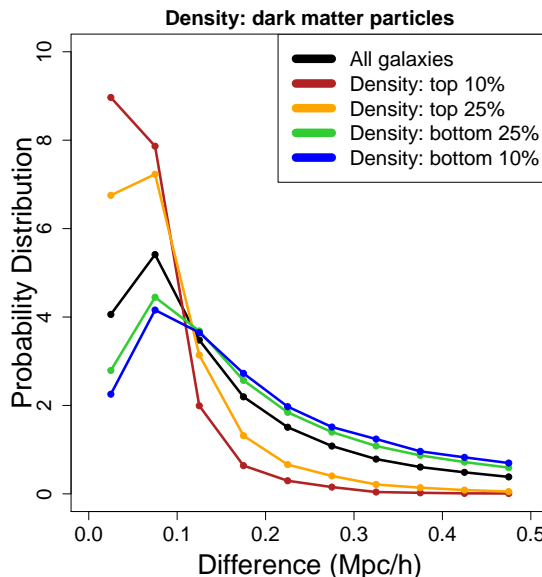


Figure 4. Agreement of filaments detected using galaxies versus using dark matter particles under different environmental densities. We rank points on filaments according to the densities of dark matter particles (using densities from galaxies yields a similar result). Then we plot distributions of filament differences under different density regimes. Filaments at high-density regions are colored by red and orange (density within the top 10% and 25%) whereas low density filaments are colored by green and blue (density in the bottom 25% and 10%). The black curve denotes the distribution using all galaxies (which is the distribution of Figure 3, note that we use the different bin size). We see a clear pattern that the two filament catalogues are similar at high-density regions and get less similar when the density decreases.

given in Figure 4. We observe that the distribution of difference for both catalogue is small, and the difference is even smaller for filaments reside in high-density regions. The reason why the difference is density-dependent is because galaxies are a biased tracer for the matter density field so that galaxies trace the large-scale structure structures better at high-density regions. Note that the result remains similar when we replace dark matter density by galaxy density.

To conclude, Figure 3 and Figure 4 show that the filaments from galaxies and the filaments from dark matter particles are similar and this similarity is stronger for high-density regions. For the following analysis on the galaxy alignment, we use the filaments from galaxies.

4.2 Principal Axes Alignment to Filaments

We first examine the correlation between principal axes and μ_F , the orientation of the nearest filament of a galaxy. Note that since both μ_j and $-\mu_j$ are describing the same axis, we take the absolute value of inner product between μ_j and μ_F .

We compute the alignment signal $|\mu_j \cdot \mu_F|$ for galaxies close to filaments ($d_F < 1$ Mpc/h) but not close to groups ($d_C > 2$ Mpc/h). Note that $|\mu_j \cdot \mu_F| \approx 1$ means that the j -th principal axis align along μ_F while $|\mu_j \cdot \mu_F| \approx 0$ indicates that they are misaligned. In Figure 5, we show the excess probability compared to the distribution of inner product between two random unit axes. We find that the alignment signal for first principal axis (blue curve) is very significant (with KS-test p-value being 4×10^{-28}). By comparing the blue curve in both the left and right side of Figure 5, we see that the distribution of the alignment is concentrated at values ≈ 1 . This means we have more aligned galaxies

compared to two galaxies with random orientations. The trend is reversed for the minor principal axis (with KS-test p-value 1×10^{-17}). Thus, we conclude that the major (first) principal axis for a galaxy tend to align along filaments while the minor axis tends to misalign to the filaments.

To study how the subhalo mass of a galaxy affects the alignment signal, we further partition galaxies by their mass into three mass-groups

$$\begin{aligned} 10^9 M_\odot/h < M < 10^{10} M_\odot/h, \\ 10^{10} M_\odot/h < M < 10^{11} M_\odot/h, \\ 10^{11} M_\odot/h < M < 10^{12} M_\odot/h \end{aligned} \quad (7)$$

and plot the average alignment signal $\langle |\mu_j \cdot \mu_F| \rangle$ within each mass bin. Note that the above three mass-groups contain 88% of all subhalos we have (about 11% of the subhalos have subhalo mass $M < 10^9 M_\odot/h$ and 0.6% have subhalo mass $M > 10^{12} M_\odot/h$). The result is given in the first two panels in Figure 6. The left (first) panel shows a clear pattern that the average alignment signal for major axis increases as the subhalo mass increases (this slope has a 4σ significance) and the effect of misalignment for minor axis is also augmented for massive galaxies. Altay et al. (2006); Zhang et al. (2009); Tempel & Libeskind (2013); Zhang et al. (2013) also report a similar mass dependency on the alignment signal.

The middle (second) panel of Figure 6 shows the same analysis as the left panel but at a different distance range to filaments. We now focus on galaxies whose distance to filaments is within $1 \text{ Mpc}/h < d_F < 2 \text{ Mpc}/h$. That is, the middle panel shows the alignment signal for galaxies that are mildly close to filaments (but not too close). Our result shows that, unlike galaxies being very close to filaments (left

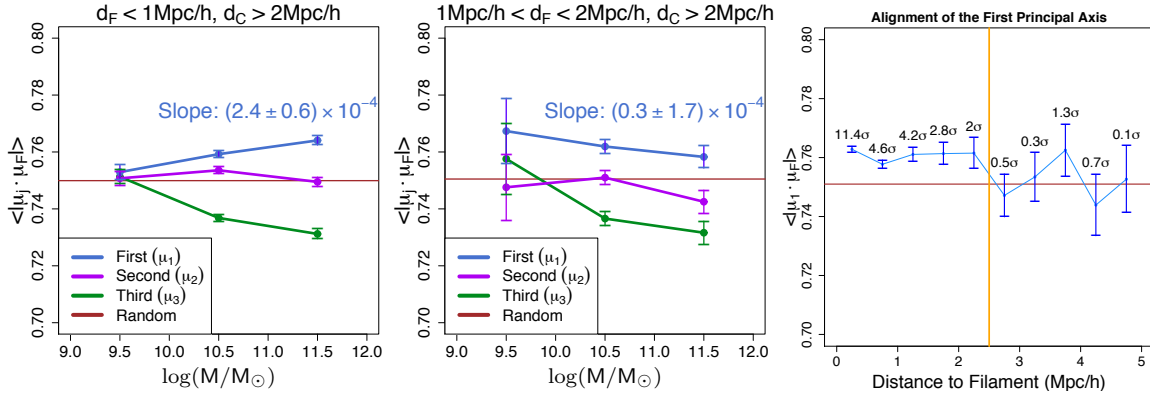


Figure 6. Alignment signals $|\langle \mu_j \cdot \mu_F \rangle|$ versus subhalo mass and d_F , the distance to filaments. Note that we remove galaxies that are close to groups (i.e. all galaxies satisfy $d_C > 2 \text{ Mpc}/h$). **Left:** We show how alignment signals change as a function of subhalo mass at $d_F < 1 \text{ Mpc}/h$. The slope of $|\langle \mu_1 \cdot \mu_F \rangle|$ versus d_F is indicated in the panel. We observe a significant (4σ) linear effect from subhalo mass on the alignment of first principal axis along the nearby filament orientation. **Middle:** The same analysis as left panel but with different range for distance to filaments ($1 \text{ Mpc}/h < d_F < 2 \text{ Mpc}/h$). Compared with left panel, we still see an alignment signal but the mass-dependency disappears. **Right:** The alignment signal for the first principal axis, $|\langle \mu_1 \cdot \mu_F \rangle|$, as a function of d_F . Note that we display the significance on top of the alignment value for each mass bin. The alignment signal is significant when $d_F < 2.5 \text{ Mpc}/h$ (left side of the orange line).

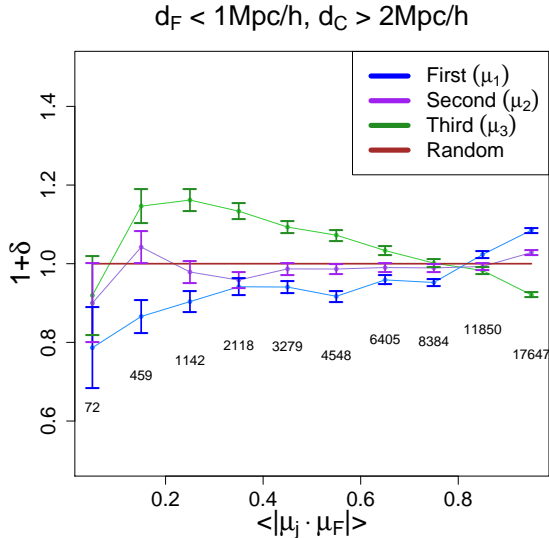


Figure 5. Distribution of alignment signals $|\langle \mu_j \cdot \mu_F \rangle|$. Note that we only consider galaxies away from groups ($d_C > 2 \text{ Mpc}/h$) but close to filaments ($d_F < 1 \text{ Mpc}/h$). We observe a significant increase for $|\langle \mu_1 \cdot \mu_F \rangle| \approx 1$. This shows that the major principal axis tend to align along the orientation of the nearby filament. The δ in the Y-axis is the excess probability compared to the distribution of random angle. The error bars are calculated from the bootstrap. The number below shows the sample size for each bin.

panel), the alignment signal is not mass-dependent (only 0.2σ).

On the right panel of Figure 6, we plot the average alignment signal for the first principal axis at different distance bins to show how the distance affects the alignment signal. Note that here we only focus on galaxy with subhalo mass between $[10^9 M_\odot/h, 10^{12} M_\odot/h]$. As expected, when the dis-

tance to filaments is small (less than $2.5 \text{ Mpc}/h$), the alignment signal is significant ($> 2\sigma$). However, when the distance is above $2.5 \text{ Mpc}/h$, we do not observe any significant alignment signal. This result is consistent with the left and middle panels of Figure 6 since the two panels both satisfy $d_F < 2.5 \text{ Mpc}/h$.

Finally, we focus on the alignment signal for first principal axis and study how the shape (q and s) influences the signal. We partition galaxies according to their q and s . The cut on q is 0.83 and the cut on s is 0.68 ; both cuts are chosen by the median value for all galaxies. The result is given in Figure 7. The left panel shows the alignment signal for the major axis under the cut on q . We find that the two groups do not have significant difference (significance is only 0.42σ). The right panel shows the same analysis under the cut on s . We see a significant difference (3.36σ) for the two groups of galaxies. Namely, an elongated galaxy (with smaller s) tends to align more along nearby filaments compared to a spherical one. This is not an effect due to measurement error since in the simulations, all the galaxies have > 500 particles and the shapes and orientations are well-measured even in the sample that are closer to round.

4.3 Principal Axes Alignment to Groups

We also study how filaments influence the galaxy alignment toward the nearest galaxy groups. We focus on the inner product between the major (first) principal axis and the direction to the nearest galaxy groups. Namely, we test how the alignment signal $|\mu_1 \cdot \mu_C|$ is different for galaxies within a filament versus outside filaments. To classify a galaxy as being inside a filament or out of filaments, we call a galaxy *in filaments* if their distance to filament d_F is less than a distance threshold τ . Otherwise, we say this galaxy is *out of filaments*. Note that we only consider galaxies that are at least $1.00 \text{ Mpc}/h$ away from the nearest group to make sure this galaxy is not in this group.

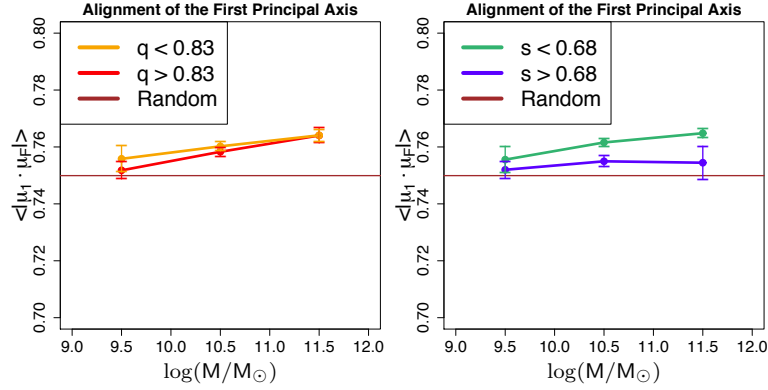


Figure 7. The correlation between shapes and the alignment signal. Note that we focus on the alignment signal of first principal axis. We study how a galaxy’s shape is correlated with $|\langle \mu_1 \cdot \mu_F \rangle|$. We split the galaxies into groups according to their shapes, measured by the q and s . The separation cuts on q and s are chosen by the median of q and s for galaxies with $d_F < 1$ Mpc/h and $d_C > 2$ Mpc/h. **Left:** We separate galaxies into two groups by q : more elliptical galaxies ($q < 0.83$, orange) and more spherical galaxies ($q > 0.83$, red). There is no significant difference between these two groups (0.42σ). **Right:** We separate galaxies into two groups by s : more elliptical galaxies ($s < 0.68$, green) and more spherical galaxies ($s > 0.68$, blue). In this case, we observe a significant difference between the two groups (3.36σ). An elliptical galaxy seems to align more along the filaments compared with a spherical one.

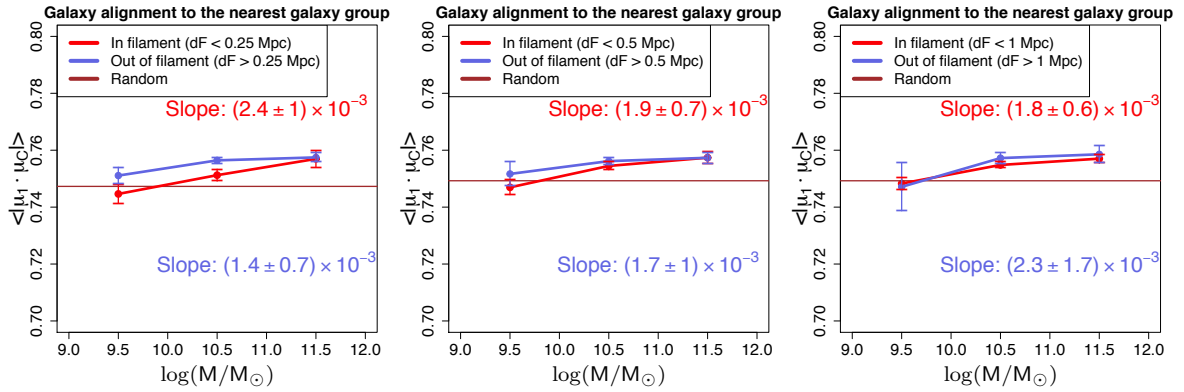


Figure 8. The effect for filaments on $|\langle \mu_1 \cdot \mu_C \rangle|$, the galaxy alignment along ‘the direction toward the nearest group’. We focus on the galaxies with $d_C > 1$ Mpc/h to make sure they are not inside a group. We then partition galaxies into two types: in filaments and out filaments by imposing a threshold τ on the distance to filaments (see § 4.3 for more details). **Left:** $\tau = 0.25$ Mpc/h. Namely, a galaxy whose distance to filaments is less than 0.25 Mpc/h will be considered *within filaments*. Otherwise this galaxy is classified as *out of filaments*. **Middle:** $\tau = 0.50$ Mpc/h. **Right:** $\tau = 1.00$ Mpc/h. The red color denotes $|\langle \mu_1 \cdot \mu_C \rangle|$ for galaxies that are inside a filament and the blue color is the same but for galaxies out of filaments. Note that we also attach the significance for the slope using the linear regression.

The result is given in Figure 8. We consider three different distance thresholds: 0.25 Mpc/h (left), 0.50 Mpc/h (middle), and 1 Mpc/h (right). In every panel, we observe that, for galaxies in filaments (red curves), the alignment signal significantly depends (the significance ranges from $2.4 \sim 3.0\sigma$) on the subhalo mass for the galaxy. On the other hand, the alignments signal for galaxies outside filaments (blue curves) are significant only when we set $\tau = 0.25$ Mpc/h but this dependency disappears for other cases. Moreover, when we increase the threshold τ , the slope (the linear effect from mass on galaxy alignments toward groups) for galaxies within filaments decreases but the slope for galaxies out of filaments increases. This suggests that the majority of the mass-dependency is from galaxies with $d_F < 0.25$ Mpc/h.

4.4 Shape Analysis

Now we study the correlation between the shape of galaxies and their proximity to galaxy groups and filaments. In particular, we focus on q for each galaxy since it measures the ratio to the length of first and second principal axis and is a useful summary statistic for the ellipticity.

We partition galaxies according to their subhalo mass into four groups:

$$\begin{aligned}
 &10^{10.0} M_\odot/h < M < 10^{10.6} M_\odot/h, \\
 &10^{10.6} M_\odot/h < M < 10^{11.0} M_\odot/h, \\
 &10^{11.0} M_\odot/h < M < 10^{11.4} M_\odot/h, \\
 &10^{11.4} M_\odot/h < M < 10^{12.0} M_\odot/h.
 \end{aligned} \tag{8}$$

Note that this partitioning is different from equation (7)

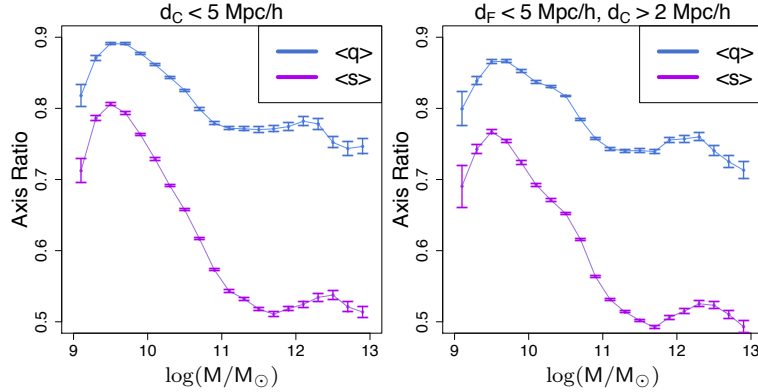


Figure 9. Impact from subhalo mass on the shapes of a galaxy. **Left:** the result for galaxies close to groups ($d_C < 5$ Mpc/h). **Right:** the result for galaxies close to filaments but not close to groups ($d_F < 5$ Mpc/h and $d_C > 2$ Mpc/h). The two distance ranges will be used in Figure 10. In both cases, we observe a strong impact on both q, s from subhalo mass.

because here we separate galaxies by subhalo mass to control the effect from subhalo mass on q . Therefore, we need a fine mass bin to reduce the mass-dependency on q . Figure 9 shows how $\langle q \rangle$ and $\langle s \rangle$ change as the subhalo mass changes. This pattern corroborates what is observed in Tennesi et al. (2014). Note that Schneider et al. (2012) observed a similar result using dark matter halos and dark matter halo shapes.

Figure 10 displays how $\langle q \rangle$ changes as d_F or d_C changes. We stack galaxies around filaments (and groups) and then partition galaxies according to their distance to filaments (and groups) into 10 bins with a bin width of 0.5 Mpc/h (so we only consider distance to filaments/groups less than 5 Mpc/h). For galaxies stacking around filaments, we have an additional constraint $d_C > 2$ Mpc/h to eliminate the effect from galaxy groups. For each bin, we also show the average subhalo mass.

Overall, we find two cases that lead to a change in the $\langle q \rangle$ after adjusting the effect from subhalo mass. The first case can be found at the top right and bottom left panel of Figure 10. We observe a decreasing pattern as d_F or d_C increases. In other words, for galaxies close to filaments or groups, we expect their q to be higher (more rounded galaxies). In both panels, the subhalo mass within each bin does not change too much so that this effect cannot be explained by the mass difference. The second case is on the difference between groups and filaments. In every panel of Figure 10, we find that, for galaxies at the same distance to either filaments or groups, $\langle q \rangle$ is always higher for galaxies close to groups.

An explanation to the above cases is due to the difference in the ratio of elliptical galaxies. If elliptical galaxies are more likely to be in/near groups and filaments and if they are usually rounder than disk galaxies, then we would expect to see that galaxies close to groups and filaments are on average rounder than those that are far away. And if this effect is stronger for groups (perhaps due to a stronger tidal field), then we should see a higher q for galaxies that are closer to groups.

Note that in the upper left panel ($10^{10.0} M_\odot/h < M < 10^{10.6} M_\odot/h$), we find a decreasing trend for the average subhalo mass when the distance to large-scale structure is increasing. Moreover, at the same distance, galaxies close to

groups tend to be lower mass compared with those close to filaments. Namely, one will find more low-mass galaxies (with subhalo mass less than $10^{10.6} M_\odot/h$) at strong tidal force regions. We do not find a similar pattern in other mass range, so this phenomena occurs only for light galaxies. A possible reason is that, in a region with strong tidal effect, matter concentrates around the large-scale structures so that there will be many newly formed galaxies. These young galaxies are generally light, which decreases the average mass.

5 CONCLUSION

In this paper, we study the correlation between galaxy orientation and filaments by applying the density ridge model to the smoothed particle hydrodynamic simulation. A short summary for what we have found is as follows:

- (i) We demonstrate that filaments constructed using density ridges from galaxy density field are similar to filaments constructed from dark matter density field. This analysis, along with the fact that density ridges are statistically consistent in both theory (Chen et al. 2015c) and simulation (Chen et al. 2015a), suggests that we might be able to reconstruct filaments of dark matter field by using only galaxies. However, this simulation goes down to quite low subhalo mass compared to most observations. More analysis needs to be done in future for real observations.
- (ii) We find that galaxies align along with their nearby filaments and this alignment is stronger for massive galaxies when the galaxy is close to filaments ($d_F < 1$ Mpc/h). This corroborates the past literature (Altay et al. 2006; Zhang et al. 2009; Tempel & Libeskind 2013; Zhang et al. 2013). Moreover, we discover that the alignment signal has a sphere of influence of 2.5 Mpc/h in radius. Namely, the principal axes of a galaxy whose distance to the nearest filaments is less than 2.5 Mpc/h would be influenced by the nearby filaments. This critical radius has not been previously reported in the literature.
- (iii) We also observe an interesting pattern: the galaxy alignment toward the nearest galaxy group is mass-dependent when this galaxy is near a filament within 0.25 Mpc/h. For

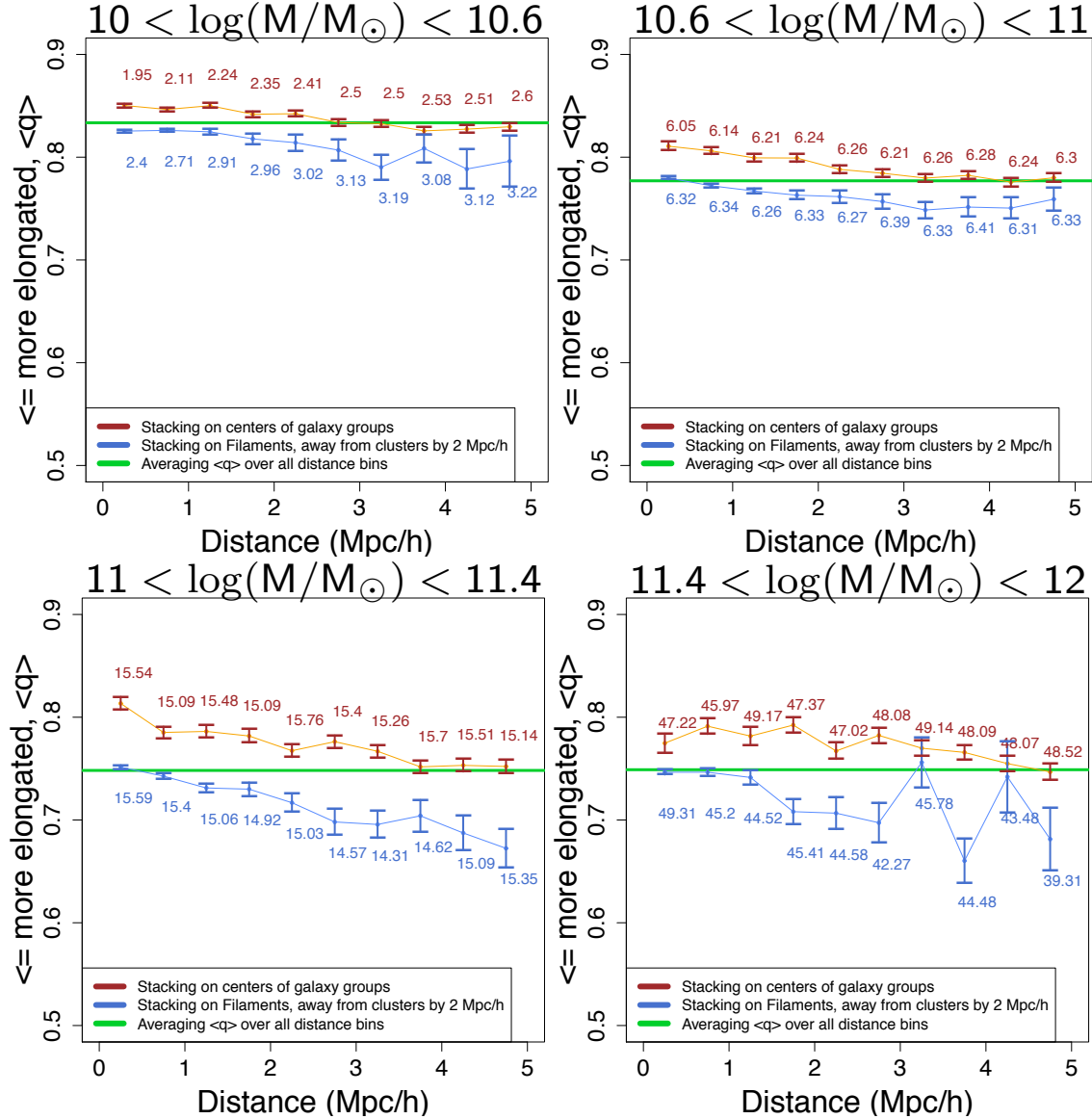


Figure 10. Influence from groups and filaments on the shape of galaxies. We display how $\langle q \rangle$ changes as the distance to filaments (blue) and groups (brown) changes. Note that we partition galaxies according to their subhalo mass to adjust the mass-dependency on $\langle q \rangle$. The number near $\langle q \rangle$ at each bin is the average subhalo mass within that bin.

galaxies close to a filament, massive galaxies tend to align along the direction toward the nearest group. For galaxies away from filaments, subhalo mass has little impact on the alignment toward a group.

- (iv) Finally, we find that the ellipticity of a galaxy is correlated with its distance to groups and filaments when the subhalo mass is between $10^{10.6}M_\odot$ and $10^{11.4}M_\odot$. A galaxy that is close to either a group or a filament tends to be less elliptical (more rounded).

The galaxy-filament alignment observed in this paper can be explained by the intrinsic alignment model and the relationship between tidal field and filaments. The intrinsic alignment model links the galaxy principal axes to the tidal field (Catelan et al. 2001; Hirata & Seljak 2004, 2010)

and the tidal field is often explicitly or implicitly used to define a filament (Hahn et al. 2007a,b; Forero-Romero et al. 2009; Cautun et al. 2013). Therefore, the principal axes and the shape of a galaxy are expected to be correlated with its nearby filament. Based on the galaxy-filament interaction we have found, we expect the future survey on intrinsic alignment and weak lensing to be improved if one incorporates the effect from filaments. This might be a way to extend the current linear or non-linear alignment model (Bridle & King 2007; Blazek et al. 2011, 2015) since the alignment along filaments can be viewed as a new type of non-linear effect.

ACKNOWLEDGMENTS

This work is supported in part by the Department of Energy under grant DESC0011114; YC is supported by DOE; SH is supported in part by DOE-ASC, NASA and NSF; AT was supported for the duration of this work by NASA ROSES 12-EUCLID12-0004. RM was supported in part by NSF under Grant. No. AST-1313169 and NASA ROSES 12-EUCLID12-0004. CG is supported in part by DOE and NSF; LW is supported by NSF.

REFERENCES

- Altay G., Colberg J. M., Croft R. A. C., 2006, *MNRAS*, **370**, 1422
- Aragon-Calvo M. A., Yang L. F., 2014, *MNRAS*, **440**, L46
- Aragón-Calvo M. A., van de Weygaert R., Jones B. J. T., 2010, *MNRAS*, **408**, 2163
- Blazek J., McQuinn M., Seljak U., 2011, *J. Cosmology Astropart. Phys.*, **5**, 10
- Blazek J., Mandelbaum R., Seljak U., Nakajima R., 2012, *J. Cosmology Astropart. Phys.*, **5**, 41
- Blazek J., Vlah Z., Seljak U., 2015, preprint, ([arXiv:1504.02510](https://arxiv.org/abs/1504.02510))
- Bridle S., King L., 2007, *New Journal of Physics*, **9**, 444
- Catelan P., Kamionkowski M., Blandford R. D., 2001, *MNRAS*, **320**, L7
- Cautun M., van de Weygaert R., Jones B. J. T., 2013, *MNRAS*, **429**, 1286
- Chen Y.-C., Genovese C. R., Wasserman L., 2014, preprint, ([arXiv:1406.1803](https://arxiv.org/abs/1406.1803))
- Chen Y.-C., Ho S., Freeman P. E., Genovese C. R., Wasserman L., 2015a, preprint, ([arXiv:1501.05303](https://arxiv.org/abs/1501.05303))
- Chen Y.-C., Genovese C. R., Ho S., Wasserman L., 2015b, preprint, ([arXiv:1506.02278](https://arxiv.org/abs/1506.02278))
- Chen Y.-C., Genovese C. R., Wasserman L., 2015c, *The Annals of Statistics*, **43**, 1896
- Crittenden R. G., Natarajan P., Pen U.-L., Theuns T., 2001, *ApJ*, **559**, 552
- Croft R. A. C., Metzler C. A., 2000, *ApJ*, **545**, 561
- Davis M., Efstathiou G., Frenk C. S., White S. D. M., 1985, *ApJ*, **292**, 371
- Di Matteo T., Colberg J., Springel V., Hernquist L., Sijacki D., 2008, *ApJ*, **676**, 33
- Di Matteo T., Khandai N., DeGraf C., Feng Y., Croft R. A. C., Lopez J., Springel V., 2012, *ApJ*, **745**, L29
- Dubois Y., et al., 2014, *MNRAS*, **444**, 1453
- Eberly D., 1996, *Ridges in Image and Data Analysis*. Springer
- Forero-Romero J. E., Hoffman Y., Gottlöber S., Klypin A., Yepes G., 2009, *MNRAS*, **396**, 1815
- Genovese C. R., Perone-Pacifico M., Verdinelli I., Wasserman L., 2014, *The Annals of Statistics*, **42**, 1511
- Hahn O., Porciani C., Carollo C. M., Dekel A., 2007a, *MNRAS*, **375**, 489
- Hahn O., Carollo C. M., Porciani C., Dekel A., 2007b, *MNRAS*, **381**, 41
- Heavens A., Refregier A., Heymans C., 2000, *MNRAS*, **319**, 649
- Heymans C., et al., 2012, *MNRAS*, **427**, 146
- Hirata C. M., Seljak U., 2004, *Phys. Rev. D*, **70**, 063526
- Hirata C. M., Seljak U., 2010, *Phys. Rev. D*, **82**, 049901
- Hirata C. M., Mandelbaum R., Ishak M., Seljak U., Nichol R., Pimbblet K. A., Ross N. P., Wake D., 2007, *MNRAS*, **381**, 1197
- Hoekstra H., Yee H. K. C., Gladders M. D., 2002, *New Astron. Rev.*, **46**, 767
- Huff E. M., Eifler T., Hirata C. M., Mandelbaum R., Schlegel D., Seljak U., 2014, *MNRAS*, **440**, 1322
- Hui L., Zhang J., 2002, preprint, ([arXiv:astro-ph/0205512](https://arxiv.org/abs/astro-ph/0205512))
- Jarvis M., Jain B., Bernstein G., Dolney D., 2006, *ApJ*, **644**, 71
- Jee M. J., Tyson J. A., Schneider M. D., Wittman D., Schmidt S., Hilbert S., 2013, *ApJ*, **765**, 74
- Joachimi B., Mandelbaum R., Abdalla F. B., Bridle S. L., 2011, *A&A*, **527**, A26
- Joachimi B., et al., 2015, preprint, ([arXiv:1504.05456](https://arxiv.org/abs/1504.05456))
- Khandai N., Di Matteo T., Croft R., Wilkins S., Feng Y., Tucker E., DeGraf C., Liu M.-S., 2015, *MNRAS*, **450**, 1349
- Komatsu E., et al., 2011, *ApJS*, **192**, 18
- Laigle C., et al., 2015, *MNRAS*, **446**, 2744
- Lee J., Pen U.-L., 2008, *ApJ*, **686**, L1
- Libeskind N. I., Hoffman Y., Forero-Romero J., Gottlöber S., Knebe A., Steinmetz M., Klypin A., 2013, *MNRAS*, **428**, 2489
- Lin H., et al., 2012, *ApJ*, **761**, 15
- Ozertem U., Erdogmus D., 2011, *JMLR*, **12**, 1249
- Pen U.-L., Lee J., Seljak U., 2000, *ApJ*, **543**, L107
- Schneider M. D., Bridle S., 2010, *MNRAS*, **402**, 2127
- Schneider M. D., Frenk C. S., Cole S., 2012, *J. Cosmology Astropart. Phys.*, **5**, 30
- Schrabback T., et al., 2010, *A&A*, **516**, A63
- Singh S., Mandelbaum R., 2014, in *American Astronomical Society Meeting Abstracts #224*. p. 423.04
- Sousbie T., Pichon C., Colombi S., Novikov D., Pogosyan D., 2008, *MNRAS*, **383**, 1655
- Springel V., Hernquist L., 2003, *MNRAS*, **339**, 289
- Springel V., White S. D. M., Tormen G., Kauffmann G., 2001, *MNRAS*, **328**, 726
- Springel V., Di Matteo T., Hernquist L., 2005, *MNRAS*, **361**, 776
- Tempel E., Libeskind N. I., 2013, *ApJ*, **775**, L42
- Tempel E., Tamm A., 2015, *A&A*, **576**, L5
- Tempel E., Stoica R. S., Saar E., 2013, *MNRAS*, **428**, 1827
- Tempel E., Guo Q., Kipper R., Libeskind N. I., 2015, *MNRAS*, **450**, 2727
- Tenneti A., Mandelbaum R., Di Matteo T., Feng Y., Khandai N., 2014, *MNRAS*, **441**, 470
- Tenneti A., Singh S., Mandelbaum R., Matteo T. D., Feng Y., Khandai N., 2015, *MNRAS*, **448**, 3522
- Troxel M. A., Ishak M., 2014, *Phys. Rev. D*, **89**, 063528
- Van Waerbeke L., Mellier Y., Hoekstra H., 2005, *A&A*, **429**, 75
- Welker C., Devriendt J., Dubois Y., Pichon C., Peirani S., 2014, *MNRAS*, **445**, L46
- Zhang Y., Yang X., Faltenbacher A., Springel V., Lin W., Wang H., 2009, *ApJ*, **706**, 747
- Zhang Y., Yang X., Wang H., Wang L., Mo H. J., van den Bosch F. C., 2013, *ApJ*, **779**, 160
- Zhang Y., Yang X., Wang H., Wang L., Luo W., Mo H. J., van den Bosch F. C., 2015, *ApJ*, **798**, 17

This paper has been typeset from a \TeX / \LaTeX file prepared by the author.